Solid-State Electronics 54 (2010) 1119–1124

Contents lists available at ScienceDirect

Solid-State Electronics

journal homepage: www.elsevier.com/locate/sse

Current injection efficiency induced efficiency-droop in InGaN quantum well light-emitting diodes

Hongping Zhao *, Guangyu Liu, Ronald A. Arif, Nelson Tansu

Center for Optical Technologies, Department of Electrical and Computer Engineering, Lehigh University, Bethlehem, PA 18015, USA

ARTICLE INFO

Article history:
Available online 11 June 2010

The review of this paper was arranged by Prof. A. Zaslavsky

Keywords:
III-Nitride
InGaN QWs
Light-emitting diodes
Efficiency-droop

ABSTRACT

Current injection efficiency and its impact on efficiency-droop in InGaN single quantum well (QW) based light-emitting diodes (LEDs) are investigated. The analysis is based on current continuity relation for drift and diffusion carrier transport across the QW-barrier system. A self-consistent 6-band $\boldsymbol{k}\cdot\boldsymbol{p}$ method is used to calculate the band structure for InGaN QW. The analysis indicates that the internal quantum efficiency in the conventional 24-Å $In_{0.28}Ga_{0.72}N$–GaN QW structure reaches its peak at low injection current density and reduces gradually with further increase in current due to the large carrier thermionic emission. Structures combining 24-Å $In_{0.28}Ga_{0.72}N$ QW with 15-Å $Al_{0.1}Ga_{0.9}N$ barriers show slight reduction in quenching of the injection efficiency as current density increases. The use of 15-Å $Al_{0.83}In_{0.17}N$ barriers shows significant reduction in efficiency-droop (10% reduction of the internal quantum efficiency at current density of 620 A/cm^2). Thus, InGaN QWs employing thin layers of larger bandgap AlInN barriers suppress the efficiency-droop phenomenon significantly.

1. Introduction

The use of *c*-plane InGaN based quantum well (QW) light-emitting diodes (LEDs) suffers from the reduction in efficiency at high operating current density, which is referred as "efficiency-droop" [1–11]. The external quantum efficiency (EQE) reaches its maximum and starts to drop at current density of 10–70 A/cm^2 [1–11]. Up to date, the origin of this phenomenon is still controversial. Various possible explanations were proposed as the mechanism for the efficiency-droop in III-nitride LEDs including: (1) carrier leakage [4–6], (2) large Auger recombination at high carrier density [10,11], (3) decreased carrier localization at In-rich regions at high injection densities [1], (4) hole transport impediment and consequent electron leakage [7,8], and (5) junction heating [2]. Approaches to enhance radiative efficiency based on novel quantum well design with enhanced optical matrix elements have been demonstrated [12–17]. However, the pursuit of novel device structures with high internal quantum efficiency up to high operating current density to address the 'efficiency-droop' still requires further investigation.

In this paper, the current injection efficiency ($\eta_{Injection}$) and internal quantum efficiency (η_{IQE}) of InGaN single-QW structures are investigated. Due to the existence of the polarization field in the InGaN QW, the band bending of the band edge potential leads to thermionic carrier escape from InGaN QW to GaN barrier regions. Due to the higher hole effective mass as compared to that of electron in nitride material, the major contribution of the carrier leakage is from the electron leakage. In this analysis, the current injection efficiency model is based on current continuity relation for drift and diffusion carrier transport across the barrier [18]. The detail of the model for current injection model for quantum well heterostructure is described in Ref. [18]. The band structure and spontaneous emission radiative recombination rate are calculated based on a self-consistent 6-band $\boldsymbol{k}\cdot\boldsymbol{p}$ method for wurtzite semiconductor [19–24].

2. Current injection efficiency and internal quantum efficiency models

The current injection efficiency ($\eta_{Injection}$) is defined as the fraction of injected current that recombine in the QW active region, and the radiative efficiency ($\eta_{Radiative}$) is the fraction of recombination current in QW that recombines radiatively. The internal quantum efficiency (η_{IQE}) can be expressed as the product of $\eta_{Injection}$ and $\eta_{Radiative}$, i.e.

$$\eta_{IQE} \equiv \eta_{Injection} \times \eta_{Radiative} \tag{1}$$

where the radiative efficiency ($\eta_{Radiative}$) is expressed as follow:

$$\eta_{Radiative} = \frac{R_{sp}}{R_{sp} + R_{non\_rad}} \tag{2}$$

In analyzing the current injection efficiency of InGaN QW, both the radiative and non-radiative recombination processes in QW

* Corresponding author. Tel.: +1 610 758 2678; fax: +1 610 758 2605.
E-mail addresses: Hoz207@Lehigh.Edu (H. Zhao), Tansu@Lehigh.Edu (N. Tansu).

0038-1101/$ - see front matter © 2010 Elsevier Ltd. All rights reserved.
doi:10.1016/j.sse.2010.05.019

and barrier regions need to be taken into account. For LED application, the current injection efficiency ($\eta_{Injection}$) can be expressed as (the details of the derivation is presented in [18]).

$$\eta_{Injection\_LED} \equiv \frac{1}{1+\frac{\tau_{BW}}{\tau_B}\cdot\left(1+\frac{\tau_{QW\_total}}{\tau_e}\right)} \tag{3}$$

From Ref. [18], the current injection efficiency of QW LEDs can be shown to depend on τ_{BW} (total carrier capture time from the barrier to QW), τ_{QW_total} (total carrier recombination lifetime in the QW), τ_e (carrier thermionic emission escape time from the QW to the barrier regions), and τ_B (total carrier recombination lifetime in the barrier regions). The schematic of the QW structure used in the analysis is similar to Fig. 1 in Ref. [18]. Note that the current analysis based on InGaN QWs takes into account the band bending due to both spontaneous and piezoelectric polarizations in the QWs. The tilting of the band lineup results in the leakage of the electrons (holes) to the *p*-type (*n*-type) GaN barrier regions. Note that the calculation of the injection efficiency assumed that sufficient electron blocking layer exist such that the drift leakage is negligible.

The parameters (τ_{QW_total}, τ_B, τ_e, τ_{BW}) described in Eq. (3) strongly depend on the carrier density. The calculation of these parameters follows the treatment in Ref. [18]. In this analysis, the calculation of the parameters τ_{QW_total} and τ_B include the calculation of both radiative carrier lifetime (τ_{Rad}) and non-radiative carrier lifetime (τ_{non_rad}). The radiative carrier lifetime (τ_{Rad}) is calculated based on the self-consistent 6-band $\boldsymbol{k}\cdot\boldsymbol{p}$ method similar to the treatment in Refs. [19–24]. The calculation of the non-radiative carrier lifetime (τ_{non_rad}) takes into consideration of both monomolecular ($A\cdot n$) and Auger ($C\cdot n^3$) recombination rates. In Eq. (2), the non-radiative recombination rate consists of both the monomolecular and the Auger recombination rates as follows:

$$R_{non\_rad} = A\cdot n + C\cdot n^3 \tag{4}$$

where A represents the monomolecular recombination coefficient and C represents the Auger recombination coefficient. The parameter n is the carrier density in QW.

The parameter τ_{BW} is composed of carrier transport time (τ_r) and quantum capture time (τ_{cap}) [18]. The carrier transport time (τ_r) is the dominant parameter, which is calculated based on the ambipolar diffusion carrier transport. The ambipolar carrier diffusion lifetime depends on the electron mobility (μ_e) and hole mobility (μ_p) for the barrier region, as well as the barrier thickness (L_s) [18]. The parameter τ_e is determined by the effective barrier height (or band offset) for both conduction band and valence band and the electron effective mass (m_e). All the parameters used in this analysis will be presented as follows.

The material parameters of nitride semiconductors employed in the calculation are obtained from Refs. [25,26]. For the calculation of the energy band gap of InGaN/AlGaN/AlInN ternaries, bowing parameters of 1.4 eV/0.8 eV [25,26]/4.1 eV [27] are used in the calculation. The band offset ratio of the conduction band to valence band (ΔE_c:ΔE_v) for GaN/InGaN, GaN/AlGaN, and GaN/AlInN are 0.7:0.3, 0.7:0.3, and 0.62:0.38 [22], respectively. The band offset ratio ΔE_c:ΔE_v for GaN/AlInN was calculated by employing model solid theory similar to the treatment in Ref. [22], where the band parameters of the AlInN ternary alloy were obtained by using the linear interpolation of the AlN and InN binary alloys. The calculation of the band offset ratio for GaN/AlInN also takes into account the valence band splitting and strain effect, similar to the treatment in Ref. [22]. For the case of $Al_{0.83}In_{0.17}N$ alloy, the lattice-matching condition will remove the strain effect.

The GaN electron mobility (μ_e) and hole mobility (μ_h) values (at T = 300 K) of 940 $cm^2/V\,s$ [28] and 22 $cm^2/V\,s$ [29] are employed in the calculation. The GaN electron effective mass value (m_e) of $0.20m_0$ is used in the calculation [25,26]. The carrier capture time (τ_{cap}) from GaN barrier into InGaN QW of 700 fs is used in the calculation [30]. In this analysis, the barrier thickness (L_s) of 10 nm is used for all of the structures. Note that values of monomolecular recombination constant (A) have been widely reported from the range of $A = 1\times10^7\ s^{-1}$ up to $A = 3\times10^8\ s^{-1}$ [4,10,31], and these discrepancies on the reported values can be attributed to the varying material quality reported by different groups. We utilize monomolecular recombination constant $A = 1\times10^7\ s^{-1}$ for InGaN QW, and the corresponding barriers (GaN, AlGaN, and AlInN layers).

The Auger recombination rate in wide bandgap III-nitride semiconductor is predicted to be significantly lower, in comparison to that of monomolecular and radiative recombination rates. Recent theoretical studies predicted Auger recombination coefficient to be $C = 3.5\times10^{-34}\ cm^6/s$ [32]. However, it is important to note that recent experimental studies have indicated the possibility that the Auger recombination coefficient in thick InGaN/GaN double heterostructure active regions (d_{Active} = 10–77 nm) in the range of $C = 1.4\times10^{-30}\ cm^6/s$ up to $C = 2\times10^{-30}\ cm^6/s$ [10,11]. Further studies are still required to clarify and confirm the Auger coefficients (C) for InGaN/GaN QW system, due to the large discrepancies from the reported Auger coefficients in the literatures [10,11,32]. Note that the Auger recombination coefficient of $C = 3.5\times10^{-34}\ cm^6/s$ from the theoretical analysis in InGaN/GaN QW system [32] was employed in this analysis.

The band structure and spontaneous radiative recombination rate (R_{sp}) calculations for the InGaN QW active regions were calcu-

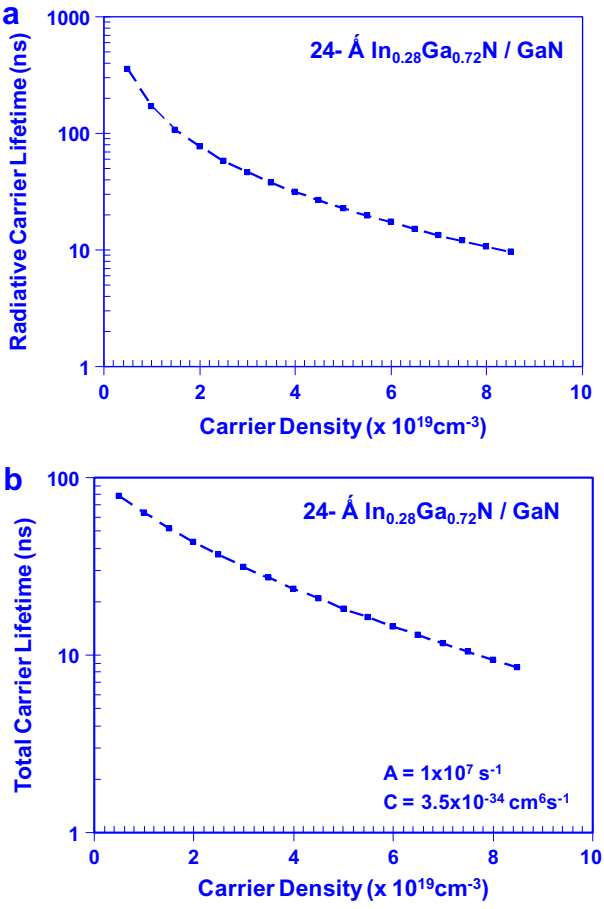

Fig. 1. (a) Radiative carrier lifetime and (b) total carrier lifetime for 24-Å $In_{0.28}Ga_{0.72}N$/GaN QW emitting at ~480 nm as a function of the carrier density up to $8.5\times10^{19}\ cm^{-3}$.

lated based on self-consistent 6-band $\boldsymbol{k}\cdot\boldsymbol{p}$ formalism for wurtzite semiconductors [19–24]. The calculation takes into account the strain effect, the valence band mixing, and the spontaneous and piezoelectric polarizations as well as the carrier screening effect. The carrier screening effect is calculated self-consistently via the Schrödinger and Poisson equations [20–24]. For the QW structures, the momentum matrix elements ($|M_{sp}|^2$) consist of both TE polarization ($|M_{TE}|^2$) and TM polarization ($|M_{TM}|^2$) components, and the spontaneous emission rate is obtained by averaging of the momentum matrix elements as follow $|M_{sp}|^2 = (2|M_{TE}|^2+|M_{TM}|^2)/3$. The details of the self-consistent numerical calculation for InGaN-based QW active regions employing 6-band $\boldsymbol{k}\cdot\boldsymbol{p}$ formalism are presented in Ref. [20].

3. Injection efficiency and IQE for InGaN/GaN QW LEDs

To calculate the internal quantum efficiency (IQE) of the InGaN–GaN QW LEDs, the radiative efficiency of InGaN QW LEDs with GaN barriers was investigated. The radiative carrier lifetime and total carrier lifetime were calculated for 480-nm emitting 24-Å $In_{0.28}Ga_{0.72}N$ QW LEDs with GaN barriers as a function of carrier density (n), as shown in Fig. 1a and b. Both radiative carrier lifetime (τ_{QW_Rad}) and total carrier lifetime (τ_{QW_total}) in InGaN–GaN QW active region decrease as carrier density increases, due to the carrier screening effect. The relatively longer carrier lifetime for InGaN-based QWs as compared to GaAs based QWs is due to the existence of the electrostatic field in InGaN QW, which leads to the spatial separation of electrons and holes. Note that the monomolecular recombination constant $A = 1\times10^{7}\ s^{-1}$ and Auger recombination coefficient $C = 3.5\times10^{-34}\ cm^6/s$ were used for the calculation of the total carrier lifetime.

To investigate the effect of current injection efficiency on efficiency-droop in conventional InGaN QW LEDs with GaN barriers, the internal quantum efficiency of the conventional structure was calculated. Fig. 2 shows the current injection efficiency ($\eta_{Injection}$) and radiative efficiency ($\eta_{Radiative}$) for 480-nm emitting 24-Å $In_{0.28}Ga_{0.72}N$ QW LEDs with GaN barriers as a function of carrier density (n). From the analysis, the current injection efficiency is relatively constant up to carrier density in the range of $n = 1.5$–$2\times10^{19}\ cm^{-3}$, however, the injection efficiency ($\eta_{Injection}$) starts to exhibit drooping phenomenon for carrier density above $n = 2\times10^{19}\ cm^{-3}$. In contrast to that, the radiative efficiency ($\eta_{Radiative}$) exhibit monotonically increasing trend as a function of carrier density.

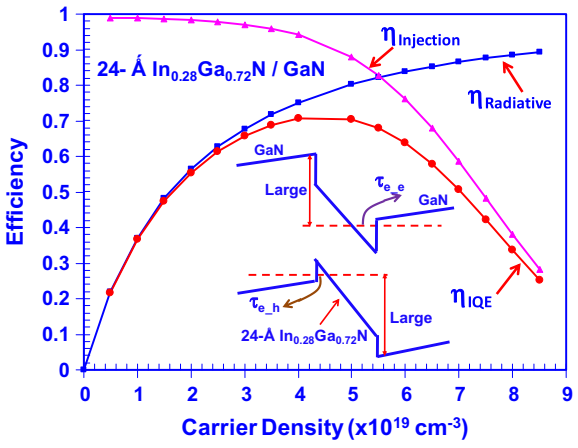

Fig. 2. IQE (η_{IQE}) of 24-Å $In_{0.28}Ga_{0.72}N$ QW surrounded by 10-nm GaN barriers ($\lambda\sim480$ nm) at 300 K. IQE (η_{IQE}), radiative efficiency ($\eta_{Radiative}$) and current injection efficiency ($\eta_{Injection}$) as a function of carrier density are plotted.

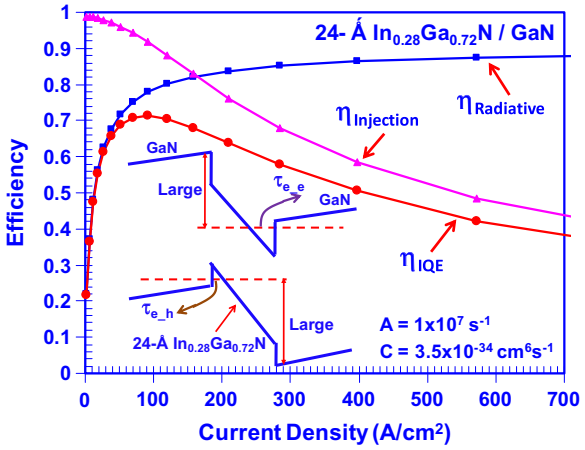

Fig. 3. IQE (η_{IQE}) of 24-Å $In_{0.28}Ga_{0.72}N$ QW surrounded by 10-nm GaN barriers ($\lambda\sim480$ nm) at 300 K. IQE (η_{IQE}), radiative efficiency ($\eta_{Radiative}$) and current injection efficiency ($\eta_{Injection}$) as a function of total current density are plotted.

Fig. 3 shows the radiative efficiency ($\eta_{Radiative}$), current injection efficiency ($\eta_{Injection}$), and the internal quantum efficiency (η_{IQE}) as a function of the total current density (J_{tot}) for 480-nm emitting 24-Å $In_{0.28}Ga_{0.72}N$ QW LEDs with GaN barriers. The thicknesses of the upper and lower GaN barrier layers are 10-nm. Note that the monomolecular recombination coefficient A of $1\times10^{7}\ s^{-1}$ and Auger recombination coefficient C of $3.5\times10^{-34}\ cm^6/s$ were used in the calculation. From Fig. 3, the radiative efficiency ($\eta_{Radiative}$) is found to rapidly increase at very low current density and approaches unity asymptotically at high current density. The injection efficiency ($\eta_{Injection}$) decreases significantly from almost unity with increasing current density. As a result, the internal quantum efficiency (η_{IQE}) increases rapidly at low current density and reaches its peak (at $n = 4\times10^{19}\ cm^{-3}$ (Fig. 2) or $J_{peak}\sim50$–$70\ A/cm^2$ (Fig. 3)) and subsequently exhibits gradual droop with increasing current injection due to the increased carrier thermionic emission. The internal quantum efficiency (η_{IQE}) is reduced to 40% of the peak value at $n = 7.5\times10^{19}\ cm^{-3}$ (Fig. 2) or $J_{tot}\sim570\ A/cm^2$ (Fig. 3).

The trend of the internal quantum efficiency for conventional InGaN QW with GaN barriers predicted by our model is in a good agreement with the experimentally-reported efficiency-droop trends in InGaN QW LEDs [8,9]. Note that the external quantum efficiency (η_{EQE}) measured from experiments [8,9] consists of both the internal quantum efficiency (η_{IQE}) and extraction efficiency ($\eta_{Extraction}$), and the extraction efficiency can be assumed as constant for varying injection current level.

Based on the finding described here, the current injection efficiency needs to be taken into account in the analysis to understand the dominant factors impacting the efficiency-droop in InGaN QW LEDs. It is also important to note that analysis or measurements without taking into account the current injection efficiency or carrier leakages could potentially lead to overestimation of Auger recombination coefficient in InGaN–GaN QW heterostructure. The understanding of the existence of carrier leakage issue in InGaN QW LEDs operating at very high current density is important for enabling potential solutions to address the efficiency-droop in nitride LEDs.

4. Approaches to suppress efficiency-droop in nitride LEDs

To suppress the efficiency-droop observed in InGaN QW LEDs, novel QW-barrier designs with significant suppression of thermionic carrier escape at high current density are required. In the proposed structure, we employed very thin layer (15-Å) larger

bandgap barrier to surround the InGaN QW active region, and these active regions are embedded in u-GaN barrier matrix. By inserting the thin (15-Å) larger bandgap barrier materials such as $Al_xGa_{1-x}N$ or $Al_xIn_{1-x}N$ to surround the InGaN QW active region, significant reduction in thermionic carrier escape rate at high current density can be achieved.

Figs. 4 and 5 show the comparison of the current injection efficiency ($\eta_{Injection}$) as a function of the carrier density (Fig. 4) and current density (Fig. 5) for 24-Å $In_{0.28}Ga_{0.72}N$ QW employing the 15-Å $Al_{0.1}Ga_{0.9}N$ barriers or 15-Å $Al_{0.83}In_{0.17}N$ barriers surrounding the QW, respectively. Low Al-content (10%) AlGaN material is slightly tensile strain with respect to GaN. The $Al_{0.83}In_{0.17}N$ material is employed in the second design due to the lattice-matching condition of this alloy to GaN. Note that the entire InGaN/AlGaN QW and InGaN/AlInN QW systems are surrounded by u-GaN layer. Both the thicknesses of the upper and lower barrier layers (u-GaN and 15-Å $Al_{0.1}Ga_{0.9}N$ or 15-Å $Al_{0.83}In_{0.17}N$) for all the structures investigated here are 10-nm, which are similar to typical barrier layers thicknesses in nitride-based LEDs grown by MOCVD. The comparison indicates that the quenching of the current injection efficiency for the InGaN/AlGaN QW LED is reduced at high carrier density or high current density, in comparison to that of InGaN–GaN QW LED. The InGaN/AlInN QW LED structure shows almost no droop up to the carrier density of $13 \times 10^{19}\,cm^{-3}$ or current density of $J_{tot} \sim 500\ A/cm^2$ due to the use of thin lattice-matched $Al_{0.83}In_{0.17}N$ ($E_g \sim 4.51$ eV) barriers.

Note that the enhancement of the injection efficiency ($\eta_{Injection}$) at high carrier density or current density for InGaN QW with thin larger bandgap barriers of AlInN or AlGaN barrier layers can be attributed to the reduction of the thermionic escape rate ($1/\tau_e$), in comparison to that of InGaN/GaN QW structure. The suppression in thermionic carrier escape rate ($1/\tau_e$) leads to enhancement of current injection efficiency, in particular up to high carrier density.

Figs. 6 and 7 show the radiative efficiency ($\eta_{Radiative}$), current injection efficiency ($\eta_{Injection}$), and the internal quantum efficiency (η_{IQE}) as a function of the carrier density (n) (Fig. 6) and total current density (J_{tot}) (Fig. 7) for 24-Å $In_{0.28}Ga_{0.72}N$/15-Å $Al_{0.1}Ga_{0.9}N$ QW, respectively. The insets of Figs. 6 and 7 show the energy band lineups for the InGaN/AlGaN QW structure, surrounded by u-GaN barrier layers. By utilizing the InGaN/AlGaN QW structure, the radiative efficiency ($\eta_{Radiative}$) is enhanced due to the enhanced spontaneous emission radiative recombination rate as compared to that of the conventional InGaN/GaN QW [20]. In addition to this, the current injection efficiency ($\eta_{Injection}$) of the InGaN/AlGaN is improved as well due to stronger thermionic carrier suppression from the use of the thin layer of higher AlGaN barrier as compared to that of the conventional InGaN/GaN QW structure. Thus, the internal quantum efficiency (η_{IQE}) for InGaN/AlGaN LEDs reaches its

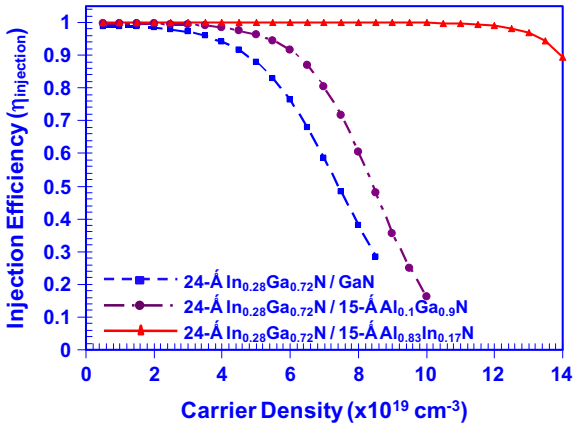

Fig. 4. Injection efficiency ($\eta_{Injection}$) as a function of carrier density for 24-Å $In_{0.28}Ga_{0.72}N$/GaN QW, 24-Å $In_{0.28}Ga_{0.72}N$/15-Å $Al_{0.1}Ga_{0.9}N$ QW and 24-Å $In_{0.28}Ga_{0.72}N$/15-Å $Al_{0.83}In_{0.17}N$ QW.

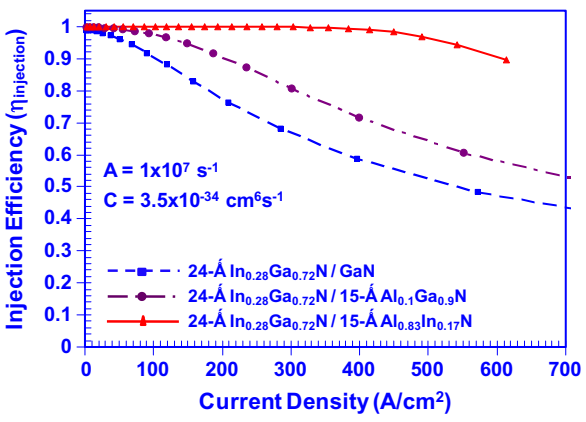

Fig. 5. Injection efficiency ($\eta_{Injection}$) as a function of total current density for 24-Å $In_{0.28}Ga_{0.72}N$/GaN QW, 24-Å $In_{0.28}Ga_{0.72}N$/15-Å $Al_{0.1}Ga_{0.9}N$ QW and 24-Å $In_{0.28}Ga_{0.72}N$/15-Å $Al_{0.83}In_{0.17}N$ QW.

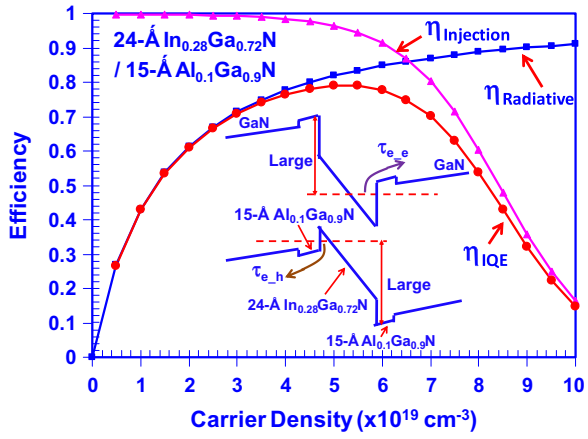

Fig. 6. IQE (η_{IQE}) of 24-Å $In_{0.28}Ga_{0.72}N$/15-Å $Al_{0.1}Ga_{0.9}N$ QW ($\lambda \sim 480$ nm) at 300 K. IQE (η_{IQE}), radiative efficiency ($\eta_{Radiative}$) and current injection efficiency ($\eta_{Injection}$) as a function of carrier density are plotted.

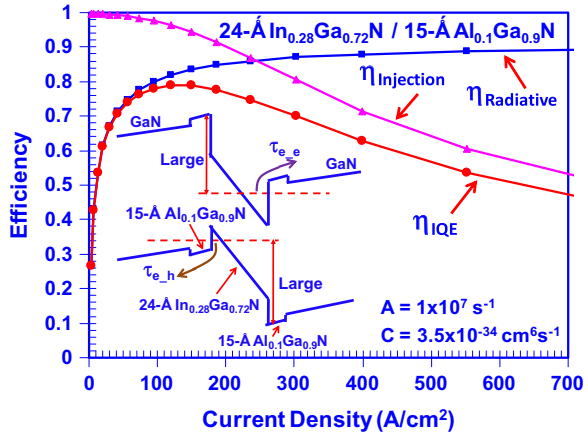

Fig. 7. IQE (η_{IQE}) of 24-Å $In_{0.28}Ga_{0.72}N$/15-Å $Al_{0.1}Ga_{0.9}N$ QW ($\lambda \sim 480$ nm) at 300 K. IQE (η_{IQE}), radiative efficiency ($\eta_{Radiative}$) and current injection efficiency ($\eta_{Injection}$) as a function of total current density are plotted.

peak at $n = 5.6 \times 10^{19}$ cm^{-3} (Fig. 6) or $J_{peak} \sim 110$–130 A/cm^2 (Fig. 7), and the IQE reduces by 32% from its peak efficiency at $n = 8 \times 10^{19}$ cm^{-3} (Fig. 6) or $J_{tot} \sim 550$ A/cm^2 (Fig. 7). The use of thin AlGaN barrier layers enables the InGaN QW LEDs to operate with higher J_{peak} and slight reduction in efficiency-droop.

Figs. 8 and 9 show the radiative efficiency ($\eta_{Radiative}$), current injection efficiency ($\eta_{Injection}$), and the internal quantum efficiency (η_{IQE}) as a function of the carrier density (n) [Fig. 8] and total current density (J_{tot}) (Fig. 9) for 24-Å $In_{0.28}Ga_{0.72}N$/15-Å $Al_{0.83}In_{0.17}N$ QW, respectively. The insets of Figs. 8 and 9 show the energy band lineups for the InGaN/AlInN QW structures, and the structures are surrounded by u-GaN barrier layers. Note that slight reduction in band bending is observed for the InGaN/AlInN QW structure, as compared to that of InGaN/GaN or InGaN/AlGaN QW-barrier structures. The electrostatic field in each layer (including the QW layer) can be calculated by considering the polarization fields in the individual layers (GaN barrier layers, thin barrier layers of AlInN or AlGaN, and InGaN QW) with periodic boundary condition, following the treatment in Refs. [20,33]. The larger polarization field in AlInN thin barrier layers, in comparison to that of GaN or $Al_{0.1}Ga_{0.9}N$ barrier layers, leads to larger electrostatic field in the AlInN layers, which in turn reduces the electrostatic field and energy band bending in the InGaN/AlInN QW-barrier structure. By utilizing the larger band gap material of AlInN as the thin barriers to surround the InGaN QW, the injection efficiency ($\eta_{Injection}$) is significantly enhanced. The use of InGaN/AlInN QW LEDs leads to injection efficiency close to unity for a large range of carrier density up to $n > 12.5 \times 10^{19}$ cm^{-3}, and this translates into high injection efficiency with very minimum droop up to current density above 500 A/cm^2. Thus, the internal quantum efficiency (η_{IQE}) of the InGaN/AlInN QW LED device starts to drop at $n \sim 12.5 \times 10^{19}$ cm^{-3} (Fig. 8) or $J_{peak} \sim 450$ A/cm^2 (Fig. 9). The internal quantum efficiency (η_{IQE}) is reduced by only 10% from its peak efficiency value at $n = 14 \times 10^{19}$ cm^{-3} (Fig. 8) or $J_{tot} \sim 620$ A/cm^2 [Fig. 9].

Note that the radiative efficiency of the InGaN/AlInN QW structure is slightly lower as compared to that of the conventional InGaN/GaN QW due to the existence of only one confined state in the QW. The use of thin AlInN barrier layer leads to stronger electron and hole confinement due to the increasing quantum size effect, which in turn leads to increase in the quantized fundamental energy levels for both electrons and holes in the QW. Due to the strong confinement and the use of thin AlInN barrier, the excited states in the conduction and valence bands of InGaN/AlInN QW structure are not confined. However, due to the much superior injection efficiency from InGaN/AlInN QW LEDs, the IQE is enhanced significantly at high operating current density.

Fig. 10a and b shows the comparison of the internal quantum efficiency (η_{IQE}) for three QW structures (24-Å $In_{0.28}Ga_{0.72}N$/GaN QW, 24-Å $In_{0.28}Ga_{0.72}N$/15-Å $Al_{0.1}Ga_{0.9}N$ QW and 24-Å $In_{0.28}Ga_{0.72}N$/15-Å $Al_{0.83}In_{0.17}N$ QW), which show the enhancement of the IQE for the QW structures with thin barrier layers of $Al_{0.1}Ga_{0.9}N$ or $Al_{0.83}In_{0.17}N$ barriers. Slight enhancement of the IQE is observed for the InGaN QW LED structure employing thin AlGaN barriers. The use of AlInN barrier layers leads to higher IQE and minimum efficiency-droop throughout a large current density range up to

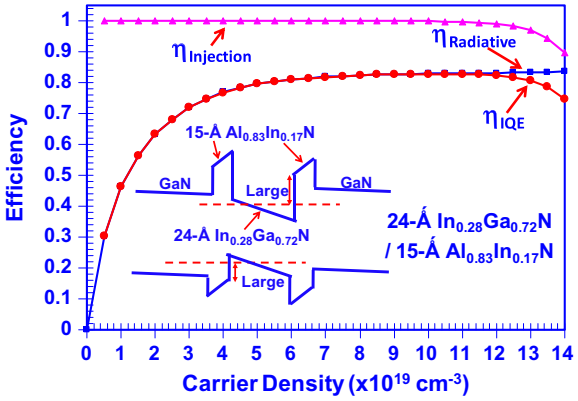

Fig. 8. IQE (η_{IQE}) of 24-Å $In_{0.28}Ga_{0.72}N$/15-Å $Al_{0.83}In_{0.17}N$ QW ($\lambda \sim 480$ nm) at 300 K. IQE (η_{IQE}), radiative efficiency ($\eta_{Radiative}$) and current injection efficiency ($\eta_{Injection}$) as a function of carrier density are plotted.

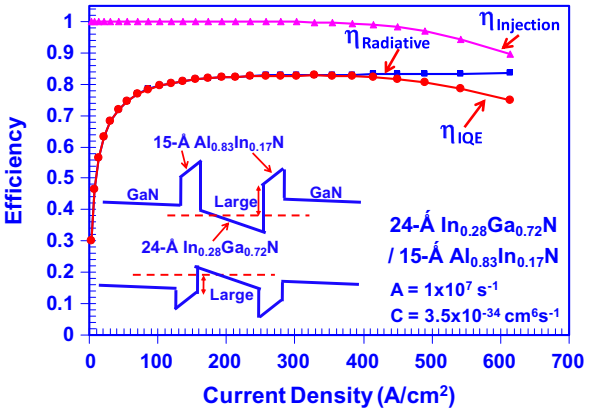

Fig. 9. IQE (η_{IQE}) of 24-Å $In_{0.28}Ga_{0.72}N$/15-Å $Al_{0.83}In_{0.17}N$ QW ($\lambda \sim 480$ nm) at 300 K. IQE (η_{IQE}), radiative efficiency ($\eta_{Radiative}$) and current injection efficiency ($\eta_{Injection}$) as a function of total current density are plotted.

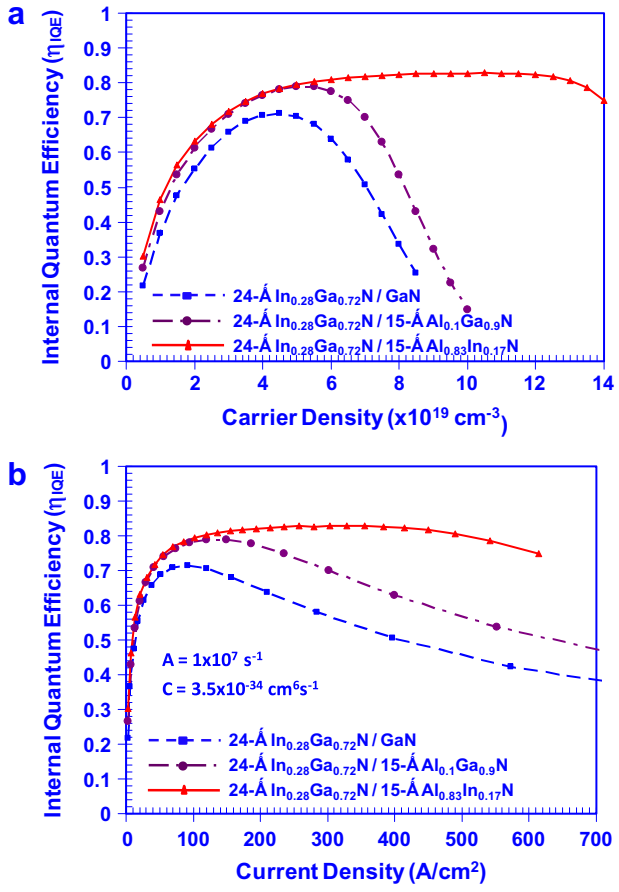

Fig. 10. IQE (η_{IQE}) as a function of (a) carrier density and (b) total current density for 24-Å $In_{0.28}Ga_{0.72}N$/GaN QW, 24-Å $In_{0.28}Ga_{0.72}N$/15-Å $Al_{0.1}Ga_{0.9}N$ QW and 24-Å $In_{0.28}Ga_{0.72}N$/15-Å $Al_{0.83}In_{0.17}N$ QW.

high current density of $J > 500$ A/cm^2. Despite the significantly superior characteristics of the InGaN/AlInN QW LEDs, further optimization on the composition and thickness of the AlInN barriers are still required. Optimization of the InGaN/AlInN QW structures with enhanced radiative efficiency ($\eta_{Radiative}$) will be important in achieving high IQE devices.

Note that the thickness of both $Al_{0.1}Ga_{0.9}N$ and $Al_{0.83}In_{0.17}N$ barriers are relatively thin (15-Å), which is important for ensuring the compatibility of the structure for epitaxy of InGaN QW LEDs. The growth of AlGaN material as barrier layer is more challenging, due to the large discrepancy of the optimized growth temperature between InGaN QW ($T_g \sim 740$ °C) and AlGaN barriers ($T_g \sim 1080$ °C) [34,35]. Thus, the use of low Al-content (10%) and very thin layers of AlGaN barriers are important for enabling the growth of high-quality InGaN/AlGaN QW structure. In contrast to that, the optimized growth condition of AlInN material is very compatible to that of InGaN QW. The optimized growth temperature for AlInN epitaxy by metalorganic chemical vapor deposition (MOCVD) ranges from $T_g \sim 750$ °C up to $T_g \sim 780$ °C [36,37], which is compatible with that of InGaN QW epitaxy.

The use of thin larger bandgap barrier material concept to suppress thermionic carrier escape had been employed for InGaAsN QW lasers with GaAsP barrier layers, resulting in very low threshold current density lasers operating up to 100 °C [18,38–40]. Based on the studies done on InGaAsN QW lasers with GaAsP barrier layers [18,38–40], there was no evidence that the use of thin barrier layers lead to injection limitation. However, further experimental studies are required to clearly understand the effect of the thin large bandgap barrier layers (i.e. AlInN), surrounding the InGaN QW, on the current/carrier injection into the QW active region.

5. Summary

In summary, we have analyzed current injection efficiency in InGaN QW and its impact on efficiency-droop for InGaN QW LEDs. The significant reduction of current injection efficiency in InGaN/GaN QW is observed at high current density, which leads to efficiency-droop issue in high-power LEDs. The utilization of thin low Al-content AlGaN layer as the QW barrier leads to slight reduction in quenching of the injection efficiency as compared to that of the conventional InGaN QW. By employing the thin layer of lattice-matched $Al_{0.83}In_{0.17}N$ barriers, the injection efficiency shows relatively minimum droop up to current density of 450 A/cm^2, which provides possible solution for the efficiency-droop issue in high-power nitride LEDs.

Acknowledgements

The authors would like to acknowledge funding supports from US Department of Energy (DE-FC26-08NT01581) and US National Science Foundation (ECCS # 0701421).

References

[1] Chichibu SF, Azuhata T, Sugiyama M, Kitamura T, Ishida Y, Okumura H, et al. J Vac Sci Technol B 2001;19(6):2177–81.
[2] Efremov AA, Bochkareva NI, Gorbunov RI, Lavrinovich DA, Rebane YT, Tarkhin DV, et al. Semiconductors 2006;40(5):605–10.
[3] Kim MH, Schubert MF, Dai Q, Kim JK, Schubert EF, Piprek J, et al. Appl Phys Lett 2007;91:183507.
[4] Schubert MF, Chhajed S, Kim JK, Schubert EF, Koleske DD, Crawford MH, et al. Appl Phys Lett 2007;91:231114.
[5] Schubert MF, Xu J, Kim JK, Schubert EF, Kim MH, Yoon S, et al. Appl Phys Lett 2008;93:041102.
[6] Xu J, Schubert MF, Noemaun AN, Zhu D, Kim JK, Schubert EF, et al. Appl Phys Lett 2009;94:011113.
[7] Xie J, Ni X, Fan Q, Shimada R, Ozgur U, Morkoc H. Appl Phys Lett 2008;93:121107.
[8] Ni X, Fan Q, Shimada R, Ozgur U, Morkoc H. Appl Phys Lett 2008;93:171113.
[9] Maier M, Kohler K, Kunzer M, Pletschen W, Wagner J. Appl Phys Lett 2009;94:041103.
[10] Shen YC, Mueller GO, Watanabe S, Gardner NF, Munkholm A, Krames MR. Appl Phys Lett 2007;91:141101.
[11] Gardner NF, Muller GO, Shen YC, Chen G, Watanabe S, Gotz W, et al. Appl Phys Lett 2007;91:243506.
[12] Park SH, Ahn D, Chuang SL. IEEE J Quantum Electron 2007;43(12):1175–82.
[13] Arif RA, Ee YK, Tansu N. Appl Phys Lett 2007;91:091110.
[14] Arif RA, Zhao H, Ee YK, Tansu N. IEEE J Quantum Electron 2008;44(6):573–80.
[15] Zhao H, Liu G, Li XH, Huang GS, Poplawsky JD, Tafon Penn S, et al. Appl Phys Lett 2009;95:061104.
[16] Zhao H, Liu G, Li XH, Arif RA, Huang GS, Poplawsky JD, et al. IET Optoelectron 2009;3(6):283–95.
[17] Park SH, Ahn D, Koo BH, Kim JW. Appl Phys Lett 2009;95:063507.
[18] Tansu N, Mawst LJ. J Appl Phys 2005;97:054502.
[19] Zhao H, Arif RA, Ee YK, Tansu N. Opt Quantum Electron 2008;40:301–6.
[20] Zhao H, Arif RA, Ee YK, Tansu N. IEEE J Quantum Electron 2009;45(1):66–78.
[21] Zhao H, Arif RA, Tansu N. IEEE J Sel Top Quantum Electron 2009;15(4):1104–14.
[22] Chuang SL, Chang CS. Semicond Sci Technol 1997;12:252–63.
[23] Chuang SL, Chang CS. Phys Rev B 1996;54(4):2491–504.
[24] Chuang SL. Physics of photonic devices. 2nd ed. New York: Wiley; 2009. p. 113–78.
[25] Vurgaftman I, Meyer JR. Nitride semiconductor devices. In: Piprek J, editor. New York: Wiley; 2009. p. 13–48.
[26] Vurgaftman I, Meyer JR. J Appl Phys 2003;94(6):3675–96.
[27] Yeh TS, Wu JW, Lan WH. J Cryst Growth 2008;310:5308–11.
[28] Farahmand M, Garetto C, Bellotti E, Brennan KF, Goano M, Ghillino E, et al. IEEE Trans Elect Dev 2001;48(3):535–42.
[29] Kozodoy P, Xing H, DenBaars SP, Mishra U, Saxler A, Perrin R, et al. J Appl Phys 2000;87(4):1832–5.
[30] Lu YC, Chen CY, Wang HC, Yang CC, Cheng YC. J Appl Phys 2007;101:063511.
[31] Son JK, Lee SN, Paek HS, Sakong T, Ha KH, Nam OH, et al. Phys Status Solidi C 2007;4(7):2780–3.
[32] Hader J, Moloney JV, Pasenow B, Koch SW, Sabathil M, Linder N. Appl Phys Lett 2008;92:261103.
[33] Bernardini F, Fiorentini V. Phys Status Solidi B 1999;216:391–8.
[34] Khan MA. Phys Status Solidi A 2006;203(7):1764–70.
[35] Kuokstis E, Sun WH, Shatalov M, Yang JW, Khan MA. Appl Phys Lett 2006;88:261905.
[36] Schenk HPD, Nemoz M, Korytov M, Vennegues P, Drager AD, Hangleiter A. Appl Phys Lett 2008;93:081116.
[37] Hernandez S, Wang K, Amabile D, Nogales E, Pastor D, Cusco R. Mater Res Soc Symp Proc 2006;892. p. 0892-FF23-04.1–6.
[38] Tansu N, Yeh JY, Mawst LJ. Appl Phys Lett 2003;83(11):2112–4.
[39] Tansu N, Mawst LJ. Appl Phys Lett 2003;82(10):1500–2.
[40] Tansu N, Yeh JY, Mawst LJ. J Phys: Condens Matter Phys 2004;16(31):S3277–318.